J Solid State Electrochem (1998) 2: 191–197

ORIGINAL PAPER

M. Soledad Ureta-Zañartu · Claudia Yáñez · Gloria Reyes
José Ramón Gancedo · José F. Marco

Electrodeposited Pt-Ir electrodes: characterization and electrocatalytic activity for the reduction of the nitrate ion

Received: 2 June 1997 / Accepted: 28 August 1997

Abstract The activity of Pt-Ir deposits on titanium for the reduction of the nitrate ion in 0.5 M perchloric acid was studied. The electrodes were characterized by SEM-EDAX, XPS and cyclic voltammetry. The activity of the electrodes for the nitrate reduction depended on the Pt-Ir ratio. Repetitive cyclic voltammograms produced an enrichment of the electrode surface with Ir and a decrease of the catalytic activity. A synergistic effect in the electrodes with low iridium content is discussed.

Key words Nitrate reduction · Bimetallic electrodes · Electrocatalysis

Introduction

Binary Pt alloys have been suggested as catalysts. Large differences in surface morphology and composition arise from the wide range of catalyst preparation methods, such as bulk alloy formation by melting or electrochemical codeposition of the elements [1]. Pt and codeposited Pt-based binary alloy electrodes have been used [2], both in industrial practice and in basic studies [3, 4]. Bimetallic Pt-Ir catalysts are used in petrochemical processing for hydrocarbon conversion and as CO oxidation catalysts for pollution control [5].

The radioactive waste from radioactive decontamination contains nitrates, nitrites, heavy metals and long-lived radionuclides [6]. The electrocatalytic reduction of nitric acid, nitric oxide [7, 8] and their derivatives [9] on different noble metal electrodes [10] and with different models of electrochemical reactors [11] has been studied. The reduction of nitrite and nitrate ions in 1 M NaOH at platinized platinum yielded ammonia at high and low overpotentials [12] respectively. Rhodium-coated electrodes show very high activities for reduction to ammonium ions [13]. Vicente et al. [14] have also reported that ammonia is formed during potentiostatic reduction of sodium nitrite solutions on a Nafion-coated Rh electrode. Nart et al. [15] have shown by FTIRS (Fourier Transform Infrared Spectroscopy) that NO_3^- ions in acid solution are readily reduced on Pt at potentials below 0.8 V, with formation of adsorbed NO. A commercial Pt-Ir alloy in 0.5 M $HClO_4$ shows an electrocatalytic activity 25 times higher than (Fourier Transform Infrased Spectroscopy) that of a Pt electrode [16]. Nitrate reduction at different electrodes [17] has been reviewed recently.

It is well known that the structure of the electrode interface influences the reaction rate [18]. The objective of this work was to prepare high-active-area Pt-Ir electrodes with a wide range of atomic compositions, obtained by electrochemical codeposition of Pt and Ir on Ti, and to evaluate their efficiency for nitrate ion reduction. The techniques of XPS, SEM-EDAX (SEM = Scanning Electrol Microscope; EDAX = Energy Dispersive Analysis; XPS = X-ray Photoelectron Spectroscopy and cyclic voltammetry (CV) were used. Ti has limited use as a cathode or cathode support because it absorbs hydrogen, which causes its mechanical deterioration. However, the rate of hydrogen absorption can be controlled by modifying the titanium surface with foreign metals [19]. Nevertheless, from an industrial point of view, titanium is more inexpensive than the platinum group metals.

M.S. Ureta-Zañartu (✉) · C. Yáñez · G. Reyes
Departamento de Ciencias Químicas, Facultad de Química y Biología, USACH, Casilla 40, Santiago-33 Chile,
Tel.: +5626820493; Fax: +5626812108
e-mail: mureta@lauca.usach.cl

J.R. Gancedo · J.F. Marco
Instituto de Química Física "Rocasolano" CSIC, Serrano 119, E-28006 Madrid, Spain

Experimental procedure

Electrode preparation

Pt and Pt-Ir films with a thickness of several μm were prepared by electrodeposition at constant current (12 to 15 mA cm^{-2}) on a Ti

substrate. Ti foils (99.7%, Aldrich) of $10 \times 10 \times 0.25$ mm^3 were washed in concentrated sulfuric acid and then pre-treated by cyclic voltammetry for 2 h in 0.5 M H_2SO_4 between −0.23 and 1.1 V (SCE), as already described [20]. In this way, through electrochemical etching, the electrodic surface remains with a very thin TiO_2 film, and therefore a better adherence of the deposit is achieved. The solutions for the deposit contained variable concentrations of hexachloroplatinic (IV) acid (acid solution about 10%, 3.8%Pt, Merck) and sodium hexachloroiridate(IV) trihydrate (99.9%, Aldrich) in 0.5 M H_2SO_4 (Merck). During the electrodeposition, a continuous stream of N_2 was passed above the previously deoxygenated solution.

Electrode characterization

The electrodes were characterized by CV in 0.5 M H_2SO_4 as already described [20]. The real electrode areas (RA) were estimated from CV curves in 0.5 M H_2SO_4 electrolyte by integration of the hydrogen adsorption (desorption) charge, assuming 220 μC cm^{-2} [21] for a monolayer of adsorbed hydrogen on iridium and 224 μC cm^{-2} on platinum [22–24].

A Pt helix of ca. 8 cm^2 was used as auxiliary electrode and a saturated calomel electrode (SCE) as reference. All potentials are referred to the SCE. Other experimental conditions have been described previously [16, 20]. The catalytic activity was measured in 0.5 M $HClO_4$. Previous studies [16] showed that nitrate reduction is a slow reaction, with competition between nitrate reduction, hydrogen adsorption and perchlorate reduction. Therefore, at room temperature, a low scan rate (5 mVs^{-1}) must be used for nitrate ion reduction to be the prevailing reaction. It is known that under certain experimental conditions the reduction of perchlorate anion occurs [17]. However, in previous studies [16] we found that with Pt and 70:30 Pt-Ir commercial alloy electrodes at room temperature, the addition to the perchlorate supporting electrolyte of a sulfate concentration equal to that of the sodium nitrate decreases the reduction rate of the nitrate ion. The catalytic activity of Ir for the reduction of ClO_4^- ion is significantly higher than that of Pt, mainly at above-ambient temperatures [25].

A JEOL scanning microscope JSM 5410 with EDAX was used. A Leybold-Heraeus LHS-10 XPS instrument with vacuum lower than 1×10^{-8} mbar, Mg Kα radiation (130 W) and an analyzer transmission energy of 50 eV was used. All the spectral spectra were recorded at take-off angles of 90°. All binding-energy values were charge-corrected using the adventitious C 1S signal at 284.6 eV. All spectra were computer fitted using known procedures [26]. Relative atomic concentrations were calculated using tabulated atomic sensitivity factors [27].

Analysis of the reaction products

The gaseous reaction products obtained by exhaustive reduction of sodium nitrate solutions by repetitive cyclic voltammetry (RCV) were analyzed in a mass spectrometer (HP 5989) coupled to a gas chromatograph (HP 5890-2) using Ar as carrier gas and for stirring the electrolyte.

Results and discussion

In recent work we found that, although the composition of a Pt-Ir bulk deposit was similar to that of the electrolyte [20], the surface composition can be influenced by the history of the electrode. According to Burke [28] et al., the formation and reduction of hydrous oxide deposits on Pt are highly irreversible, which was attributed to the influence of the lattice coordination number (or stabilization energy) of surface metal atoms. Therefore we carried out XPS and SEM measurements both on fresh electrodes and with electrodes that had been cycled for 2 h in 0.5 M $HClO_4$. The different Pt-Ir electrodes are labeled according to the Pt-Ir proportion in the electrolyte.

SEM results

SEM images of different Pt-Ir co-deposits show a homogeneous distribution of bright spots on a dark background (see Fig. 1). EDAX reveals that the contents of Ir and Pt in the bright spots is much higher than that of the background, where the titanium signal from the substrate predominates. The images in Fig. 1A, B and C reveal fewer dark sites and greater homogeneity in the deposit at lower iridium contents. The presence of separate phases for Pt and Ir is unlikely, although the phase diagram for Pt:Ir at room temperature presents a region of total immiscibility [20, 29]. Repetitive potential cycling for 2 h broke the electrodeposit and even caused scaling of the titanium foil (see Fig. 1D) (compare Figs. 1A and 1D, both with a 30:70 Pt:Ir electrolyte in the deposit cell). At a higher magnification (see Figs. 1E and 1F), the deposits treated by RCV show flakes 1–2 mm thick and cavities containing grains smaller than those on the surface.

XPS results

Figure 2A shows the Ir 4f and Pt 4f signals of a fresh electrode. Since the Pt 4f peaks are close to the Ir 4f peaks, the fit of the Ir 4f and Pt 4f signals was done simultaneously. Thus, the spectrum was best-fitted to four spin-orbit doublets. The binding energy values, the relative percentages of the different chemical species and the Pt/Ir atomic ratios are given in Table 1. The most important contribution to the Pt 4f spectrum corresponds to the spin-orbit doublet characterized by the binding energies of the $4f_{7/2}$ and $4f_{5/2}$ levels of 70.9 eV and 74.3 eV, respectively. These values are characteristic of Pt metal [30–32]. The binding energies of the Pt $4f_{7/2}$ and Pt $4f_{5/2}$ levels corresponding to the second Pt 4f spin-orbit doublet are 72.8 eV and 75.9 eV, respectively. These values are similar to those shown by Pt^{2+} compounds such as PtO or $Pt(OH)_2$ [14]. The Ir 4f spectrum also shows two contributions (i.e. two spin-orbit doublets). The peaks corresponding to the main contribution are located at 62.4 eV and 65.4 eV and are similar to those shown by Ir^{4+} species [33]. The peaks corresponding to the second Ir 4f doublet appear at 60.3 eV and 63.1 eV and are characteristic of Ir metal [17]. After potential cycling (Fig. 2B), there is a clear enhancement of the Ir 4f peaks compared with the Pt 4f peaks (see also Table 1).

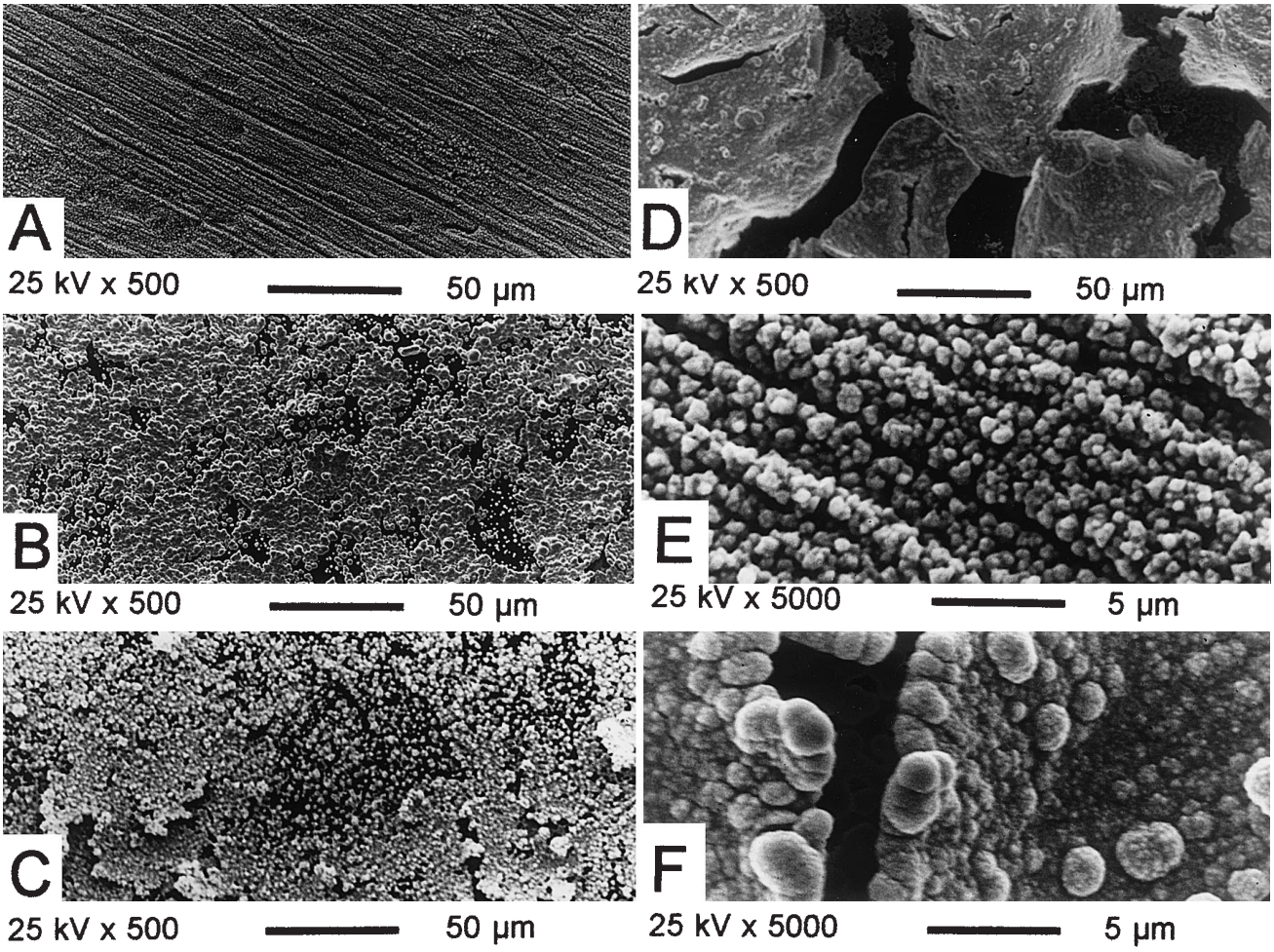

Fig. 1A–F SEM images of Pt-Ir codeposits on Ti foil. **A** 70:30 Pt:Ir, **B** 50:50 Pt-Ir, **C** 30:70 Pt-Ir, **D** same sample as **A** but after potential cycling, **E** same as **A** but at higher magnification, and **F** same sample as **D** but at higher magnification

The Ir 4f spectrum continues to show both the Ir metal and the Ir^{4+} contributions, but the Pt 4f spectrum shows only the Pt metal contribution. If a second Pt 4f contribution is included in the fitting procedure, too small linewidths (less than 1.0 eV) are obtained. If the linewidth of this second contribution is fixed to that obtained for the Pt^{2+} species of the fresh electrode, a very small relative intensity (less than 3%) and a large chi squared value are obtained.

The background at high binding energies of the Pt 4f spectrum obtained after potential cycling has a negative slope (positive if the kinetic energy scale is considered) as compared with that of the spectrum of the fresh electrode, which is characteristic of a layer buried under a thin overlayer [34]. Furthermore, the energy loss tail height (i.e. the ratio of the intensity across the peak to the height of the peak at its maximum) is about the same for the Pt and Ir 4f peaks of the fresh electrode, while it is much larger for the Pt 4f peaks than for the Ir 4f peaks in the cycled electrode. This is an indication of a deeper location within the surface of the Pt phase than that with in the Ir phase [35]. Taken together, all the results indicate that potential cycling produces an Ir enrichment of the electrode surface. This is discussed below.

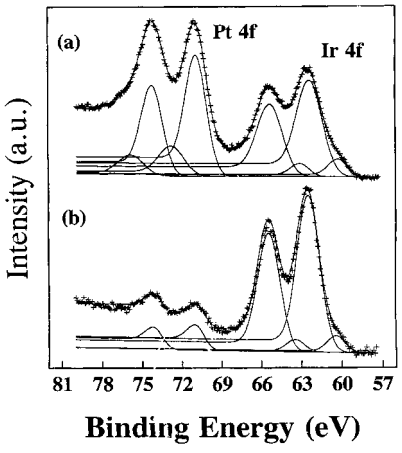

Fig. 2a, b XPS Pt 4f and Ir 4f spectra of 70-30 Pt-Ir codeposits on Ti foil. **a** Fresh codeposit and **b** repetitive potential cycling

Table 1 Binding energies and ratios obtained from the fit of the XPS spectra shown in Figure 2a and b.

Sample	Energy (eV)	Element/Line	Assignment
Pt-Ir	60.3	$Ir/4f_{7/2}$	Ir metal
fresh	63.1	$Ir/4f_{5/2}$	
	62.4	$Ir/4f_{7/2}$	Ir^{4+}
	65.4	$Ir/4f_{5/2}$	
	70.9	$Pt/4f_{7/2}$	Pt metal
	74.3	$Pt/4f_{5/2}$	
	72.8	$Pt/4f_{7/2}$	Pt^{2+}
	75.9	$Pt/4f_{5/2}$	
ratios:		$Ir^{4+}/Ir = 7.33$	
		$Pt^{2+}/Pt = 0.3$	
		$Pt_{total}/Ir_{total} = 1.2$	
Pt-Ir	60.5	$Ir/4f_{7/2}$	Ir metal
cycled	63.5	$Ir/4f_{5/2}$	
	62.5	$Ir/4f_{7/2}$	Ir^{4+}
	65.5	$Ir/4f_{5/2}$	
	71.1	$Pt/4f_{7/2}$	Pt metal
	74.2	$Pt/4f_{5/2}$	
ratios:		$Ir^{4+}/Ir = 8.7$	
		$Pt_{total}/Ir_{total} = 0.12$	

Cyclic voltammetry results

Figure 3 shows CVs at 100 mV/s in 0.5 M $HClO_4$ of codeposited Pt-Ir electrodes and of the pure metals. With electrodes that contain Ir, the positive limit was 0.86 V to avoid a possible dissolution of Ir, whose superficial oxides are more soluble than those of platinum. The current densities, referred to the geometric area, are not fully comparable because of differences in surface roughness. In Fig. 3, the real active areas (RA) of the electrodes are indicated. The CVs of Pt-Ir codeposits have Pt-like structures down to relatively low amounts of Pt in the electrodeposit solution. The CV of the electrodeposit does not show the typical reversible surface process of massive Ir [36], in agreement with the reports that the oxides of electrodeposited Ir are more irreversible than those of massive Ir [37, 38]. Note that for similar electrodeposit conditions, the amount of deposit decreases with increasing concentration of iridium in the solution. The current efficiency of iridium electroplating is rather low, particularly at room temperature [37]. Upon increasing the Ir content above 50%(w/w) a decrease of RA is observed.

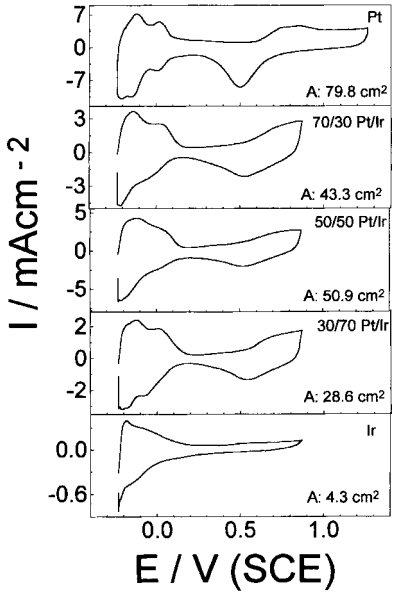

Fig. 3 Cyclic voltammograms of different Pt-Ir codeposits in 0.5 M $HClO_4$ at 5 mV/s. RA is the real active area (see text)

Cyclic voltammetries of nitrates reduction were run between 0.3 and −0.23 V, starting at 0.3 V. Nitrate ions block the surface, this blocking being lifted by cycling between −0.23 and 0.86 V.

Figure 4 shows CVs at 5 mVs^{-1} in 0.5 M $HClO_4$ + x M $NaNO_3$ solutions for four Pt-Ir electrodes. The reduction of nitrate starts in the double-layer region and produces a cathodic peak in the negative scan. In the reverse (positive) scan another cathodic peak appears, as observed for a 70:30 Pt:Ir commercial alloy [16]. The intensity of the cathodic peak current (I_p) increases with increasing $[NO_3^-]$ (Fig. 4). Nitrate shifts the hydrogen evolution to more negative potentials. The cathodic current increases with the concentration of nitrate, but reaches saturation for $[NO_3^-] = 0.2$ M independently of the amount of iridium in the electrode. This saturation was also found with a 70:30 Pt:Ir commercial alloy [16]. The curves belonging to 50:50 Pt:Ir at $E > 0.1$ V yield low cathodic currents during the positive scan in the absence of NO_3^- ions, the distortion of the voltammetric curves being perhaps due to ClO_4^- reduction. Studies carried out in our laboratory with iridium electrodes showed that sulfate ions inhibit both the nitrate and perchlorate reduction, and that at room temperature the reduction of ClO_4^- is slower than that of NO_3^-.

The effect of ageing of a 70-30 Pt-Ir codeposited electrode on its catalytic activity was studied by repetitive

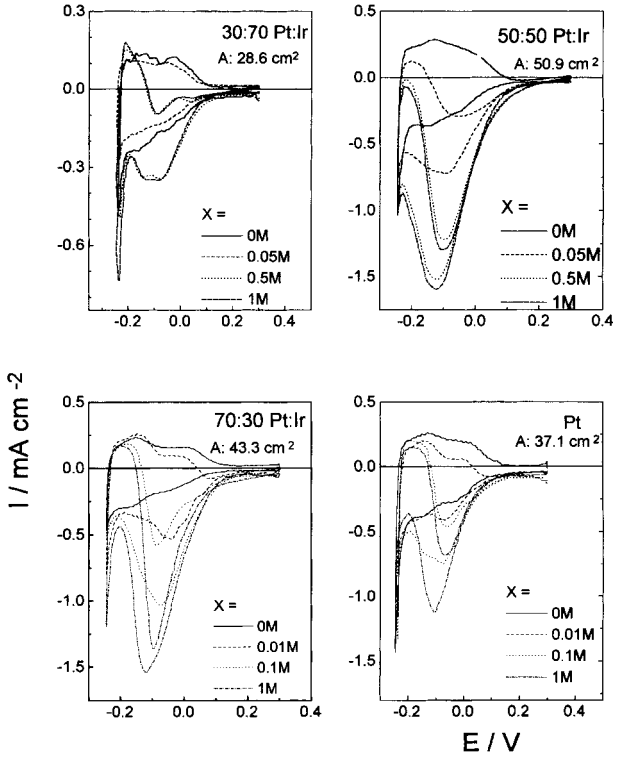

Fig. 4 Effect of the concentration of nitrate ion on the CV at 5 mV/s of different Pt-Ir codeposits in 0.5 M $HClO_4$ + x M $NaNO_3$. RA is the real active area

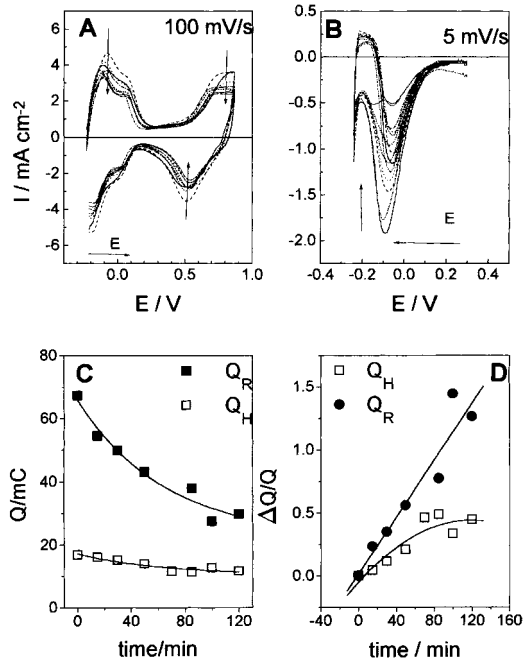

Fig. 5A–D Ageing of the 70:30 Pt-Ir electrode by repetitive potential cycling for 2 h. The *vertical arrows* indicate the sense of decrease of I (cathodic) with the number of scans and *horizontal arrows* the sense of the first scan. **A** CVs with different numbers of previous scans in 0.5 M $HClO_4$, **B** same as **A** but with 0.1 M $NaNO_3$, **C** plot of charge densities of hydrogen desorption (Q_H) obtained from CV at 5 mV/s in 0.5 M $HClO_4$ and nitrate reduction (Q_R) obtained from plot **B**, with "time" correspond to cycling time and proportional to number of scans, and **D** plot of $\Delta Q/Q$ for Q_H and Q_R vs time

potential cycling at 100 mVs^{-1} in 0.5 M $HClO_4$ in the presence and absence of nitrate. To evaluate the electrode activity, CVs at 5 mVs^{-1} between 0.3 and −0.23 V were run. Without nitrate, a decrease in the current density with cycling time is observed, as indicated by the arrows in Fig. 5A. The hydrogen desorption charge (Q_H) (Fig. 5C) shows a decrease in the first cycles only, perhaps due to a loss of deposit and/or to a decrease of the roughness (or porosity) of the electrode. The activity (Fig. 5B) also decreased in both scan directions. Cycling shifts the peak potentials towards less negative values and causes a new cathodic peak to appear at more negative potentials. The reduction charge densities (Q_R) associated with these CVs have been plotted in Fig. 5C. The decrease in Q_R is greater than that expected according to the decrease in Q_H ($\Delta Q_R/Q_R \gg \Delta Q_H/Q_H$, see Fig. 5D), and, since Q_H values for Ir and Pt are almost the same, the decrease in Q_H can be attributed to changes in surface atomic roughness, but the decrease in Q_R can be related to partial dissolution of the deposit layers. These results are in good agreement with those obtained by XPS, which show that RCV produces an Ir enrichment of the surface. Since the Pt/Ir ratio is 1.2 for a fresh electrode and 0.12 for the electrode treated by RCV (see Table 1), the Q_R decrease is related to the iridium enrichment of the surface. Furthermore, it should be emphasized that for a fresh electrode the Ir^{4+}/Ir ratio is 7.3 as against 8.7 for the treated electrode, and $\Delta Q_R/Q_R \gg \Delta Q_H/Q_H$, which indicates that some of the iridium that diffuses to the surface from the bulk is present as iridium-oxygen compounds, where Ir is in a higher oxidation state and some is dissolved.

The finding that an increase in the concentration of iridium in the deposit is associated with a decrease of the electrocatalytic activity can be explained only if iridium is present as an irreversible oxide. Impedance studies of massive iridium electrodes have shown differences between activated and unactivated electrodes [39], attributed to a higher concentration of active sites in the first case. Kötz et al. [40], using XPS, postulated that the loss of activity of electrodeposited Ir is probably associated with dissolution of the hydrous Ir oxides at the outer layer and exposure of the "inner compact" oxide close to the titanium surface. Čukman and Vuković [37] could not activate iridium on an electrodeposited electrode previously stabilized by thermal treatment (freezing). They observed a decrease in the oxide formation charge in the second positive scan, which was not accompanied by a corresponding decrease of the cathodic charge of oxide reduction. Pt^{2+} was not detected in cycled electrodes with the last sweep towards negative potentials, which indicates that Pt behaves reversibly. These results, together with the decrease in Q_H, suggest that during cycling there is a rearrangement in the deposit structure and that also a partial dissolution, preferentially of iridium, probably takes place.

In order to compare the activity of the electrodes, we use the parameter $\{-(I-I^{\circ})/\mathrm{RA}\}$, where I and I° are the peak currents in CVs at 5 mVs^{-1} in the presence and absence of 1 M $NaNO_3$, respectively, and RA is the real electrode area (see Fig. 4). Figure 6A shows curves obtained during the ageing process. Only one reduction peak (at −0.1 V), whose height decreases with the cycling time, is observed. In Fig. 6B curves of the same class for new electrodes (recently prepared) with different Pt-Ir proportion are shown. It is observed that electrodes with less than 50% Ir are more active than the Pt electrode. However, an electrode with 70% Ir is practically inactive. The electrocatalytic activity of 70:30-Pt:Ir aged electrode is greater than that of deposited Pt (Fig. 6).

Since nitrite could act as a catalyst of nitrate reduction [16], experiments in the presence of nitrite were made with a 70:30-Pt:Ir codeposit in 0.5 M $HClO_4$. Fig. 7A shows CVs in the presence and absence of both 0.1 M NO_3^- and 10^{-3} M NO_2^-. A smaller $[NO_2^-]$ was used because nitrite is more active than nitrate at a Pt electrode [41]. Increasing additions of a 10^{-3} M NO_2^- solution show an increase in I_p with $[NO_2^-]$ (Fig. 7B) for small nitrite additions only. The saturation observed indicates that nitrite ion catalyzes the reduction of nitrate through reactions such as:

$$HNO_2 + H^+ \rightarrow NO^+ + H_2O \quad (1)$$

$$NO^+ + NO_3^- \rightarrow N_2O_4 \quad (2)$$

in which the N_2O_4 molecule can give N_2O or NO_2 as the final product and begin a new cyclic process as proposed previously. As Ir adsorbs OH at lower potentials than Pt, it is likely that this process occurs through the reaction

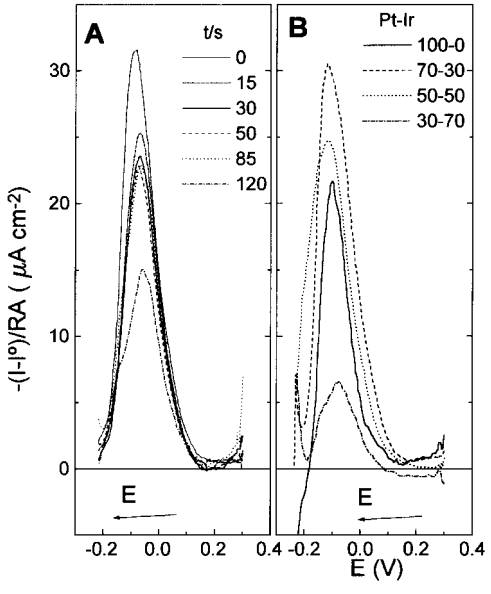

Fig. 6 Plot of $-(I-I^{\circ})/\mathrm{RA}$ vs E for **A** different times of treatment by RCV on 70:30 Pt-Ir electrode and **B** different Pt-Ir codeposits. I and I° are the currents in the negative scan, at 5 mV/s, in 0.5 M $HClO_4$ with and without 1 M $NaNO_3$, respectively

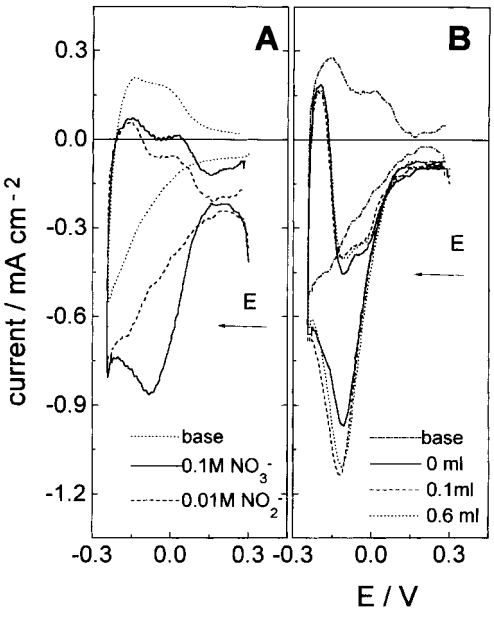

Fig. 7 Effect of the nitrite ion in voltammograms at 5 mV/s with a 70-30 Pt-Ir electrode in **A** 0.5 M $HClO_4$ and **B** 0.5 M $HClO_4$ + 0.1 M $NaNO_3$

$$Ir + H_2O \rightarrow Ir\text{-}OH + H^+ + e \quad (3)$$

facilitating the cleavage of the water molecule and thus giving the superficial H^+ necessary for the reaction of Eq. 1, as proposed in [16].

The reaction gases during cycling (0.3 → −0.23 V) with a 70-30 Pt-Ir electrode in 0.5 M $HClO_4$ + 0.5 M $NaNO_3$ were collected by Ar bubbling. Since the electrode becomes poisoned with adsorption residues [16] and with cycling, it was cleaned by cycling between −0.23 and 0.86 V, gas collection being stopped during this cleaning. N_2 was the main reaction product ($m/e = 28$); small signals at $m/e = 44$ and $m/e = 17$ were attributed to N_2O and NH_3, respectively. These results are in agreement with those of Enyo et al. [42] and Gootzen et al. [43], who detected N_2O at potentials lower than 0.4 V vs RHE.

Conclusions

Porous Pt, Ir, and Pt-Ir electrodes were made by galvanostatic deposition on Ti foil substrates. The results obtained in this work indicate that nitrate reduction occurs at a higher rate on 70:30 Pt-Ir electrodes than on pure Pt. The role played by Ir in Pt-Ir electrodes is that of a bifunctional heterogeneous catalyst, i.e. a synergetic effect in which the electrode has a higher activity than the sum of those of the components. Thus, iridium promotes the adsorption of OH in a reversible, more reactive form, and Pt promotes the adsorption sites for nitrogenous species.

It is important to emphasize that the current densities of the electrodes are not fully comparable because of slightly different degrees of surface roughness. The current densities referred to the geometric area are higher for Pt-Ir electrodes than for deposits of the individual metals, probably because of a greater porosity of the codeposit; electrodes with Ir between 30 and 50 per cent have the higher hydrogen areas. On the other hand, in spite of the "ageing effects", the Pt-Ir electrodes obtained by electrolytic codeposition are more active than either metal in separate form, and their high (active area/geometric area) ratio makes them interesting for water treatment systems. The method of cleaning the poisoned electrodic surface is very easy: it suffices to vary the sweep potential limits.

Perhaps it would be interesting to submit the codeposited bimetallic electrodes to different thermal treatments in different atmospheres in order to achieve more stable, rougher surfaces. However, if the baking temperature is too high, the electrode surface can be deactivated by dehydration, as occurs with repetitive cyclic voltammetry.

Acknowledgements This work was supported by DICYT-USACH (grant 9641UZ) and FONDECYT (grant 1930093). C. Yáñez is grateful to CONICYT for a Doctoral Fellowship.

References

1. Friederich KA, Geyzers KP, Linke U, Stimming U, Stumper J (1996) J Electroanal Chem 402: 123
2. Chu D, Gilman S (1996) J Electrochem Soc 143: 1685
3. Markovic NM, Gasteiger HA, Ross PN, Jiang X, Villegas I, Weaver MJ (1995) Electrochim Acta 40: 91
4. Poirier JA, Stoner GE (1995) J Electrochem Soc 142: 1127
5. Wagner FE, Sawicki JA, Bolton JH (1988) Hyperfine Interactions 41: 733
6. Coleman DH, White RE, Hobbs DT (1995) J Electrochem Soc 142: 3815
7. Otsuka K, Sawada H, Yamanaka I (1996) J Electrochem Soc 143: 3491
8. Rodes A, Gómez R, Pérez JM, Feliu JM, Aldaz A (1996) Electrochim Acta 41: 729
9. Kudo A, Mine A (1996) J Electroanal Chem 408: 267
10. Horányi G, Wasberg M (1997) Electrochim Acta 42: 261
11. Prasad S, Weidner JW, Farell AE (1995) J Electrochem Soc 142: 3815
12. Genders JD, Hartsough D, Hobbs DT (1996) J Appl Electrochem 26: 1
13. Wasberg M, Horanyi G (1995) Electrochim Acta 40: 615
14. Vicente F, García-Jareño JJ, Cervilla A, Domenech A (1995) Electrochim Acta 40: 1121
15. Da Cunha MCPM, Weber M, Nart FC (1996) J Electroanal Chem 414: 163
16 Ureta-Zañartu MS, Yáñez C (1997) Electrochim Acta 42: 1725
17. Spivey JJ (1996) Electrosorption studies in electrocatalysis (Catalysis, A specialist periodical report, vol 12). The Royal Society of Chemistry
18. Trasatti S (1995) Surface Sci 335: 1
19. Trasatti S (1992) In: Gerischer H, Tobias CW (eds) Advances in electrochemical science and engineering, vol 2. VCH, New York, p 1
20. Ureta-Zañartu MS, Yáñez C, Páez M, Reyes G (1996) J Electroanal Chem 405: 159
21. Ortiz R, Márquez OP, Márquez J, Gutiérrez C (1996) J Phys Chem 100: 8389
22. Beden B, Hahn F, Leger JM, Lamy C, Perdriel CL, de Tacconi NR, Lezna RO, Arvía AJ (1991) J Electroanal Chem 301: 129
23. Trasatti S, Petrii OA, (1992) J Electroanal Chem 327: 353
24. Bockris JO'M, Jeng KT (1992) J Electroanal Chem 330:541
25. Sánchez-Cruz M, González-Tejera MJ, Villamañan MC (1985) Electrochim Acta 30: 252
26. Sherwood PMA (1990) In: Briggs D, Seah MP (eds) Auger and X-ray photoelectron spectroscopy (practical surface analysis, 2nd edn, vol 1). Wiley, Chichester, p 574
27. Wagner CD, Davis LE, Zeller MV, Taylor JA, Raymond RM, Gale LH (1980) Surf Interf Anal 2: 222
28. Burke LD, Buckley DT (1995) J Appl Electrochem 25: 913
29. ASM Handbook (1992) Alloy Phase Diagram, vol 3, ASM International, The Materials Information Society, New York, p 266
30. Hammond JS, Winograd N (1977) J Electroanal Chem 78: 55
31. Peuckert M, Bonzel HP (1984) Surf Sci 145: 239
32. Peuckert M, Coenen FP, Bonzel HP (1984) Electrochim Acta 29: 1305
33. Augustyninski J, Koudelka M, Sánchez J, Conway BE (1984) J Electroanal Chem 160: 1305
34. Watts JF (1994) Vacuum 45: 653
35. Castle JE, Ke R, Watts JF (1990) Corros Sci 30: 771
36. Ureta-Zañartu MS, Bravo P, Zagal J (1992) J Electroanal Chem 337: 241
37. Cukman D, Vukovic M (1990) J Electroanal Chem 279: 283
38. Boodts JCF, Trasatti S (1989) J Appl Electrochem 19: 255
39. Ferrer JE, Victori Ll (1994) Electrochim Acta 39: 667
40. Kötz R, Neff H, Stucki S (1984) J Electrochem Soc 131: 72
41. Petrii OA, Safonova TYa (1992) J Electroanal Chem 331: 897
42. Nishimura K, Machida K, Enyo M (1991) Electrochim Acta 36: 877
43. Gootzen JFE, Van Hardeveld RM, Visscher W, van Santen RA, van Veen JAR (1996) Recl Trav Chim Pays-Bas 115: 480